ARTICLE OPEN

Check for updates

Terahertz lattice and charge dynamics in ferroelectric semiconductor $Sn_xPb_{1-x}Te$

Y. Okamura[1]✉, H. Handa[1], R. Yoshimi[2], A. Tsukazaki[3], K. S. Takahashi[2], M. Kawasaki[1,2], Y. Tokura[1,2,4] and Y. Takahashi[1,2]✉

The symmetry breaking induced by the ferroelectric transition often triggers the emergence of topological electronic states such as Weyl fermions in polar metals/semimetals. Such strong coupling between the lattice deformation and electronic states is therefore essentially important for the control of versatile topological phases. Here, we study the terahertz lattice and charge dynamics in ferroelectric semiconductor $Sn_xPb_{1-x}Te$ thin films hosting versatile topological phases by means of the terahertz time-domain spectroscopy. With lowering the temperature, the resonant frequency of transverse optical (TO) phonon shows the significant softening and upturn. This temperature anomaly of lattice dynamics directly indicates the displacive-type ferroelectric transition. The resulting phase diagram suggests the enhancement of ferroelectricity in the films possibly due to compressive strain compared with the bulk crystals. The low-energy TO phonon induces the large DC and terahertz dielectric constant even in metallic state. Furthermore, we find that the Born effective charge of phonon mode is enhanced at around the compositions showing the band gap closing associated with the topological transition.

npj Quantum Materials (2022)7:91 ; https://doi.org/10.1038/s41535-022-00501-2

INTRODUCTION

Ferroelectrics, which spontaneously break the space inversion symmetry, have been investigated as one of the most fundamental phases of matter from the early stage of condensed matter physics[1]. So far, many ferroelectric materials and their unique physical properties such as the giant dielectric response, piezoelectric effect, and softening of transverse optical (TO) phonon have been extensively explored. The ferroelectrics now play a crucial role in today's device engineering such as capacitors and memories. Recently, the concept of polar metal expands the field of materials science. The ferroelectrics are usually considered to be characteristic of insulators, since the metallicity and ferroelectricity tend to be mutually exclusive with each other because the static internal electric field is screened by itinerant electrons. The progress in materials search has developed this new class of materials in this decade as exemplified by $LiOsO_3$[2], carrier-doped perovskite titanates[3,4] and transition metal dichalcogenides[5,6], while such a phase was originally predicted by a seminal theoretical work in 1960s[7]. These materials show intriguing phenomena related to both the charge and lattice dynamics such as ultrafast structural control by intense carrier acceleration[8] and enhanced thermopower near the boundary of the polar-to-nonpolar phase transition[9]. These findings suggest that the interplay between charge and lattice dynamics potentially provides the versatile physical properties in polar metals. In particular, the softening of TO phonon in displacive-type ferroelectrics, which signals the structural instability and causes the enhanced dielectric response, is an intriguing target. However, the study on the dielectric properties of soft TO phonon in metals has been hardly addressed so far because the response of conduction electron overlaps with the low-energy dielectric response of TO phonon.

$Sn_xPb_{1-x}Te$ crystallizing in a rocksalt structure is the well-known IV-VI semiconductor exhibiting the ferroelectric instability (Fig. 1a). The electronic states of these compounds recently attract revived interests due to the appearance of topological phases depending on the composition x[10–12]. SnTe is known to be the topological crystalline insulator with polar distortion along <111> axes, which often shows the metallic conduction due to the Sn vacancy. The inelastic neutron and x-ray scattering measurements reveal the presence of the soft phonon at the Brillouin zone center below 4 meV, demonstrating the displacive-type ferroelectric transition[13,14]. It is suggested that the ferroelectric transition temperature strongly depends on the carrier concentration in SnTe[15]. On the other hand, PbTe is the trivial insulator with good thermoelectric performance under appropriate doping[16,17]. This material is also known as the incipient ferroelectric exhibiting the strong anharmonicity of optical phonon and local symmetry breaking, although the detailed nature is still controversial[18–21]. Inbetween the topological crystalline insulator for SnTe and trivial insulator for PbTe, the Weyl semimetallic state shows up with help of inversion symmetry breaking as suggested by the anomalous Hall and Nernst signals arising from the Weyl nodes in momentum space[22–26]. These studies indicate that the composition variation as well as the external pressure can induce the dramatic difference in the (topological) electronic and lattice states. The terahertz optical spectroscopy can directly measure the resonance of soft TO phonon and the conduction electron dynamics in the energy range of meV, providing an insight into the enhanced dielectric response associated with the structural instability in the topological semimetallic phase.

Here we investigate the terahertz lattice and charge dynamics of polar semiconductor $Sn_xPb_{1-x}Te$ thin films ($x = 0$, 0.16, 0.30, 0.43, 0.63, 0.80, and 1) by means of terahertz spectroscopy. The fabrication of thin films enables the fine composition tuning, leading to the control of the ferroelectricity. In the terahertz conductivity spectra, we observe the clear phonon excitation for all the compositions as well as the electronic continuum band except for insulating PbTe ($x = 0$). The phonon excitations show

[1]Department of Applied Physics and Quantum Phase Electronics Center, University of Tokyo, Tokyo 113-8656, Japan. [2]RIKEN Center for Emergent Matter Science (CEMS), Wako 351-0198, Japan. [3]Institute for Materials Research, Tohoku University, Sendai 980-8577, Japan. [4]Tokyo College, University of Tokyo, Tokyo 113-8656, Japan.
✉email: okamura@ap.t.u-tokyo.ac.jp; youtarou-takahashi@ap.t.u-tokyo.ac.jp

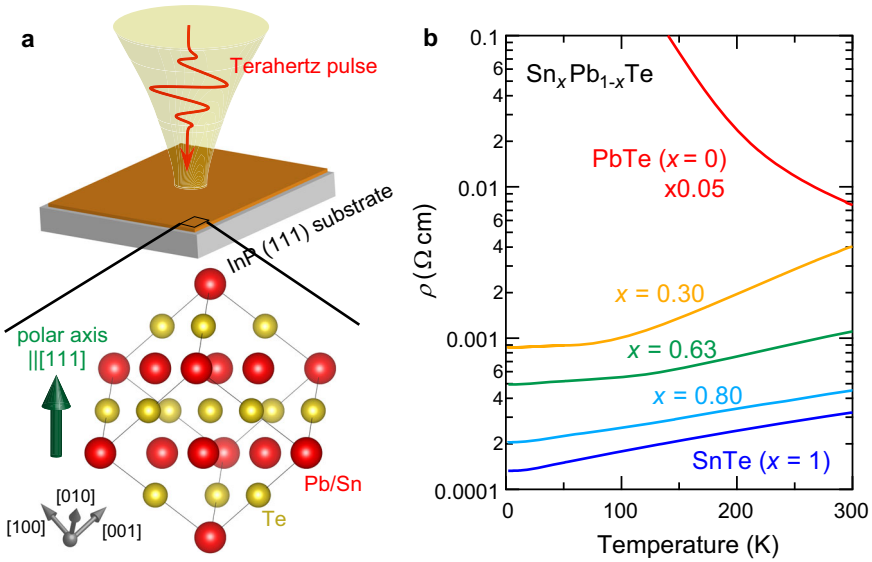

Fig. 1 Crystal structure and transport property of $Sn_xPb_{1-x}Te$ thin films. a Crystal structure of $Sn_xPb_{1-x}Te$. The thin film was fabricated on InP (111) substrate. The polar axis along the out-of-plane [111] direction is inferred from the second harmonic generation in the previous study[25]. The terahertz light is incident normal to the plane. **b** The temperature dependence of the resistivity for $Sn_xPb_{1-x}Te$ ($x = 0$, 0.30, 0.63, 0.80, 1).

the softening with decreasing temperature and then clear hardening for $0.16 \le x \le 0.80$. This observation indicates the robust ferroelectric transition under the presence of conduction electrons. The established putative phase diagram suggests the stabilization of the ferroelectricity compared to the bulk system most likely due to the strain from substrate. The low-energy phonon induces the enhanced DC dielectric constant. The enhancement of Born effective charge of TO phonon shows the clear correlation with the band gap closing.

RESULTS

Sample and characterization

We used the high-quality (111)-oriented (Sn,Pb)Te epitaxial thin films with 2-nm thick SnTe buffer layer fabricated on InP(111)A substrate by molecular beam epitaxy (Fig. 1a; see also Methods). Figure 1b summarizes the temperature dependence of the resistivity of $Sn_xPb_{1-x}Te$ thin films for $x = 0$, 0.30, 0.63, 0.80, and 1 which we used in the present terahertz measurement. The longitudinal resistivity ρ exhibits the systematic composition x dependence ranging over four orders of magnitude at 2 K; PbTe ($x = 0$) shows the semiconducting or insulating behavior while Sn-doped samples tend to show the metallic behavior. The Hall resistivity measurement in the previous work confirmed that Sn-substitution induces p-type carriers[25]. The appearance of polar axis along the out-of-plane [111] direction has been indicated by the optical second harmonic generation (SHG) even for thin film PbTe, while PbTe in the bulk form is paraelectric (Fig. 1a). This suggests the stabilization of ferroelectricity in the present thin film form.

Terahertz spectra

We measured the terahertz conductivity and dielectric spectra by using the terahertz time-domain spectroscopy in the transmittance geometry (for details, see Methods). The terahertz spectra represent only the in-plane response for the normal incidence of the terahertz light. It should be emphasized that the terahertz measurement on thin films enables the quantitative evaluation of dielectric response of optical phonons, which directly reflects the emergence of ferroelectricity, even for the metallic samples. In bulk form, the metallic sample makes the measurement of terahertz spectra difficult owing to their reflectivity approaching unity.

The in-plane optical conductivity spectra Re $\sigma(\omega)$ for each composition are shown in Fig. 2. In PbTe (Fig. 2a), a peak of TO phonon exhibits clear softening with decreasing the temperature, indicating the development of lattice instability close to the ferroelectric phase transition. When substituting Pb with Sn, the continuum band due to the electronic excitation shows up in addition to the resonance of TO phonon. With increasing the Sn concentration x or decreasing the temperature, the electronic continuum is increased in accord with the reduction in resistivity (Fig. 1b); Re $\sigma(\omega)$ in the lowermost energy well coincides with the DC conductivity obtained from the transport measurement which gives Re $\sigma(\omega = 0)$ as shown by circles at zero energy (Fig. 2b–e). The phonon peak becomes unclear at the highly conductive regions, for example, SnTe at 5 K (purple curve in Fig. 2e).

To look into the phonon dynamics, we analyze the observed $\sigma(\omega)$ under the assumption that the terahertz response is composed of the electronic response $\sigma^{ele}(\omega)$ and phonon response $\sigma^{ph}(\omega)$ (see also Supplementary Note 1 for fitting function). As an example, we show the fit to the terahertz spectra for $Sn_{0.30}Pb_{0.70}Te$ at 5 K in Fig. 3 (purple curve in Fig. 2b) by using the following formula;

$$\sigma(\omega) = \sigma^{ele}(\omega) + \sigma^{ph}(\omega) = \sigma_0 + i\omega\varepsilon_0\left(1 - \varepsilon(\infty) - \varepsilon^{ph}(\omega)\right) \quad (1)$$

with

$$\varepsilon^{ph}(\omega) = \frac{S_{ph}\omega_T^2}{\varepsilon_0\left(\omega_T^2 - \omega^2 - i\omega\gamma\right)} \quad (2)$$

ε_0, $\varepsilon(\infty)$, ω_T, S_{ph} and γ are the dielectric constant of vacuum, dielectric constant in high-frequency limit, TO phonon energy, phonon's oscillator strength and damping constant, respectively. Here, we assume that $\sigma^{ele}(\omega)$ in the present energy window (1 – 8 meV) can be regarded as the lower-lying tail of the intraband/interband electronic excitation and approximated to be a frequency-independent constant value σ_0 because the DC conductivity is almost the same as Re $\sigma^{ele}(\omega)$ at $\hbar\omega = 8$ meV. The overall feature of the real and imaginary parts of the terahertz conductivity spectra is well reproduced by Eq. (1) (Fig. 3a, b). σ_0 almost coincides with the DC conductivity (green curves). The resonance structure due to the phonon excitation shows the

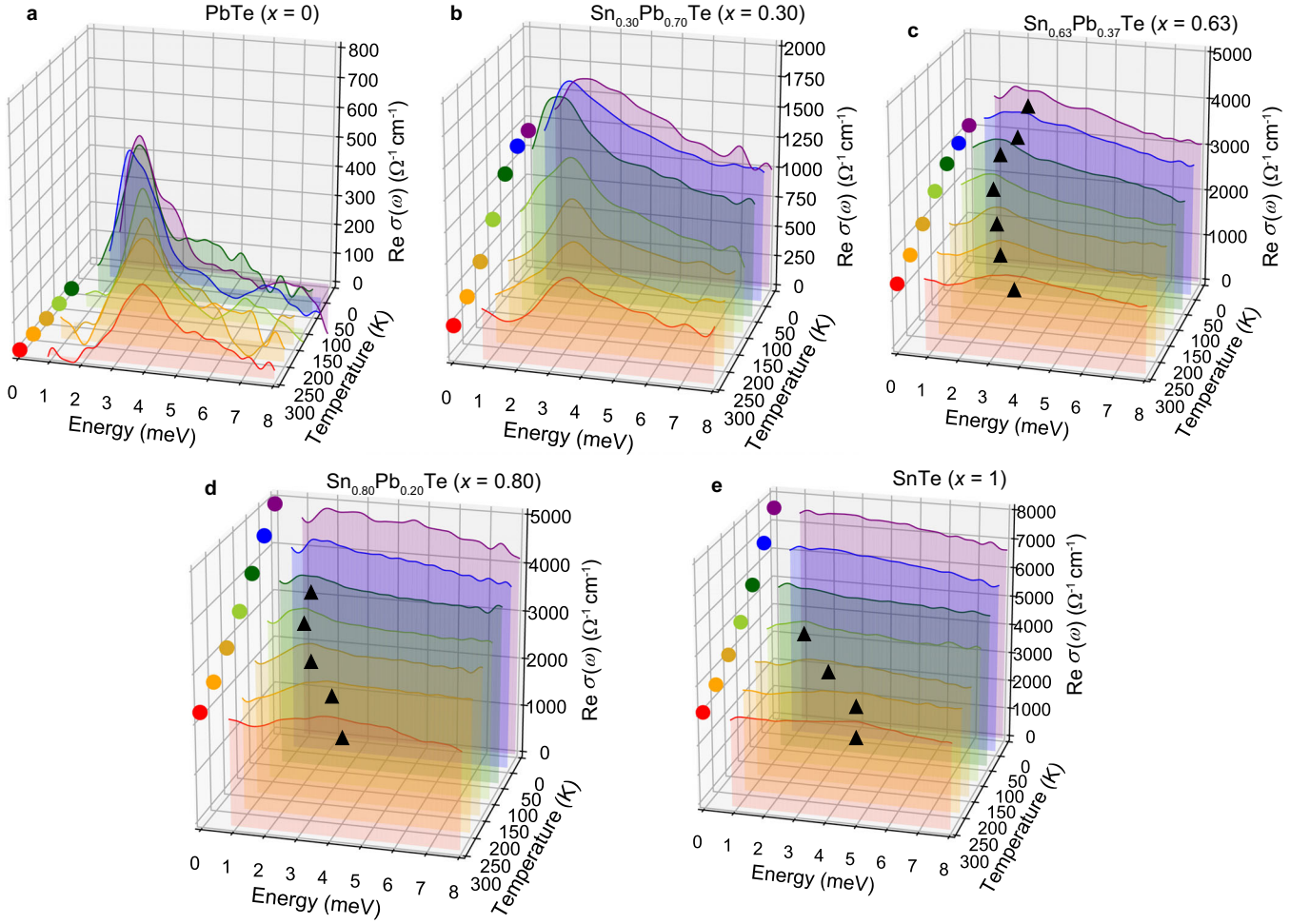

Fig. 2 Terahertz conductivity spectra of $Sn_xPb_{1-x}Te$ thin films. a–e Temperature dependence of the real part of the optical conductivity spectra Re $\sigma(\omega)$ for $Sn_xPb_{1-x}Te$ ($x = 0$, 0.30, 0.63, 0.80, 1). The filled circles in zero-energy planes represent the DC conductivity obtained from the transport measurement. The data at 5 K (purple), 50 K (blue), 100 K (green), 150 K (yellow green), 200 K (ocher), 250 K (orange) and 300 K (red) are plotted. In (**c**–**e**), the phonon excitations are indicated by black triangles for clarity.

resonance-type and dispersion-type spectra in Re $\sigma^{ph}(\omega)$ and Im $\sigma^{ph}(\omega)$, respectively (light blue curves). In a similar manner, other spectra shown in Fig. 2 can be decomposed into the resonant peak of TO phonon and flat continuum stemming from conduction electron except for the highly conductive regime, i.e., the Sn-rich compositions ($x = 0.80$, 1) at low temperatures. In these regions, the Drude-like behavior is indicated by the zero-energy peak in Re $\sigma(\omega)$; in case of SnTe at 5 K (purple curve in Fig. 2e), for example, Re $\sigma(\omega)$ shows the gradual decrease as a function of energy, where the scattering rate multiplied by $\hbar$ is estimated to be 23 meV.

The dielectric spectra obtained from the experiment and above fitting procedure are summarized in Fig. 4a–e. The real part of the dielectric spectra can be transformed from the optical conductivity spectra as,

$$\mathrm{Re}\,\varepsilon(\omega) = 1 - \frac{\mathrm{Im}\,\sigma(\omega)}{\varepsilon_0\omega} = \mathrm{Re}\,\varepsilon^{ph}(\omega) + \varepsilon(\infty) - \frac{\mathrm{Im}\,\sigma^{ele}(\omega)}{\varepsilon_0\omega} \quad (3)$$

Here we can omit $\varepsilon(\infty)$ and Im $\sigma^{ele}(\omega)$ in Eq. (3), because $\varepsilon(\infty)$ is as small as 40 for the present system[27,28], being negligible as compared to the $\varepsilon^{ph}(\omega)$, and Im $\sigma^{ele}(\omega)$ is nearly zero in most cases as observed in the aforementioned $Sn_{0.30}Pb_{0.70}Te$ case (Fig. 3b). In fact, the observed Re $\varepsilon(\omega)$ is well reproduced only by the theoretical Re $\varepsilon^{ph}(\omega)$ (dotted curves in Fig. 4a–e). The dispersive structures with large amplitude manifest the enhanced dielectric response of TO phonon. The DC dielectric constant arising from the TO phonon $\varepsilon^{ph}(0)$ tends to be enhanced as the phonon softens at low temperatures (open circles, Fig. 4f–j); for example, it exceeds 2000 for the $x = 0.30$ compound (see open circles in Fig. 4g). This enhanced $\varepsilon(0)$ is consistent with the Lyddane-Sachs-Teller (LST) relation, $\varepsilon(0)/\varepsilon(\infty) = \omega_L{}^2/\omega_T{}^2$, in which the resonance energy of the longitudinal optical (LO) phonon, ω_L, is as large as 17 meV[29,30].

Ferroelectric phase diagram

The TO phonon energy ω_T obtained from fits with Eqs. (1) and (2) is plotted for each composition as a function of temperature (filled circles in Fig. 4f–j). With decreasing the temperature, the TO phonon shows the significant softening for all the compositions down to the certain temperature, which is defined as T_C. The clear softening is observed even in metallic SnTe, being consistent with the previous inelastic x-ray scattering[14]; the screening effect does not affect the emergence of ferroelectricity at least in the present carrier density ($\sim 6\times10^{20}\,\mathrm{cm}^{-3}$ for SnTe)[15]. The frequency lowering down to the T_C can be well described by the Curie Weiss law, $\omega_T \propto \sqrt{T - T_C^*}$ (dotted curves in Fig. 4f–j; see Fig. 4g for the definition of T_C and T_C^* as an example).

Below the T_C, the temperature dependence of the phonon energy shows the clear upturn in case of $x = 0.30$, 0.63 and 0.80 (Supplementary Fig. 2). It is to be noted that the observed TO

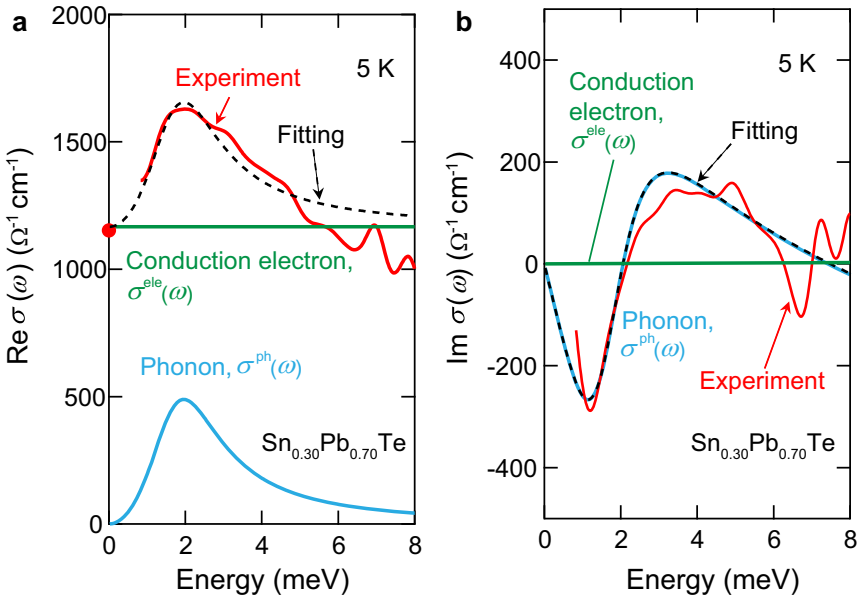

Fig. 3 Decomposition of the terahertz conductivity spectra into the electronic and phonon responses. Real (**a**) and imaginary (**b**) parts of $\sigma(\omega)$ at 5 K for $Sn_{0.30}Pb_{0.70}Te$. Red solid, green solid, light blue solid and black dashed curves represent the experimental spectrum, electronic continuum band $\sigma^{ele}(\omega)$, phonon response $\sigma^{ph}(\omega)$ and fitting spectrum, respectively. The red filled circle at zero energy at (**a**) denotes the DC conductivity obtained from the transport measurement.

phonon has different polarization from the TO phonon causing the ferroelectric transition. The TO phonons are triply degenerated in the cubic paraelectric state and one of them is randomly frozen in the ferroelectric state in a bulk crystal. In the thin film, the three modes are split into two in-plane polarized unfrozen modes observed here and one out-of-plane polarized frozen mode causing the ferroelectric transition at T_C due to the epitaxial strain. It is well known that the soft phonon polarized along the polar direction shows the steep hardening below the ferroelectric transition temperature[31]. The unfrozen phonon modes polarized perpendicular to the polar direction show weaker hardening through the anharmonic coupling with other displacement modes allowed by the symmetry breaking in the Landau free energy[31,32]. This behavior of soft phonon is generally observed in many materials possessing the degenerated soft phonons such as perovskite ferroelectrics[31]. Therefore, although the observed in-plane polarized TO phonon is not the true soft phonon that has triggered the out-of-plane polarity below the transition temperature, we can reasonably ascribe the upturn of the phonon energy observed in Fig. 4g–i to the signature of the ferroelectric transition, being also consistent with the enhanced SHG at low temperatures[25]. Likewise, in case of $x = 0$, while the temperature dependence of phonon energy shows the weaker anomaly, the deviation from the Curie Weiss law can be ascribed to the ferroelectric transition as suggested by the enhancement of SHG signal at low temperatures[25].

In Fig. 5a, we show the putative ferroelectric phase diagram of $Sn_xPb_{1-x}Te$ thin film deduced from the terahertz spectroscopy. Both T_C^* and T_C tend to increase with increasing the Sn concentration x as observed in the bulk system[15,33,34]. Meanwhile, the transition temperature for the present thin film system is much enhanced compared to the bulk system, demonstrating the stabilization of the ferroelectric phase. This might be attributed to the compressive strain from substrate promoting the elongation along the out-of-plane [111] direction, while the presence of strain field is not clear at least within the experimental accuracy of the x-ray diffraction at room temperature[25].

Enhanced Born effective charge

We discuss the oscillator strength of the optical phonons in terms of Born effective charge. The dielectric response of TO phonon in Eq. (2) can be described by explicitly using the Born effective charge Z^* as,

$$\varepsilon^{ph}(\omega) = \frac{N(Z^*e)^2}{M^*\varepsilon_0}\frac{1}{\omega_T^2 - \omega^2 - i\omega\gamma}, \quad (4)$$

where N, e and M^* represent the oscillator density, elementary charge and reduced mass, respectively. The Z^* for PbTe and SnTe are respectively estimated to be ~ 5.2 and ~ 5.3, both of which are much larger than the formal valence of Pb or Sn ion 2+. These enhanced Z^* are roughly consistent with the first-principles calculation showing $Z^* = 6.16$ for PbTe and $Z^* = 8.26$ for SnTe (blue squares, Fig. 5b)[34].

Notably, the Z^* shows the appreciable enhancement up to ~ 8 at around $x \simeq 0.3$ (Fig. 5b and Supplementary Fig. 3), at which the appearance of Weyl semimetal phase is suggested in the bulk system[23,26]. The enhanced mobility and SHG also imply the possible Weyl semimetallic state around $x \simeq 0.16$ in the present film[25]. The enhancement of Z^* indicates a significant electronic contribution rather than ionic origin. To see the relation to the electronic states, we focus on the $\varepsilon(\infty)$ connected to the Born effective charge through the LST relation; $Z^* \propto \varepsilon(\infty)(\omega_L^2 - \omega_T^2)$, where phonon frequencies $(\omega_L^2 - \omega_T^2)$ less affect Z^* because the ω_L shows little composition dependence ($\omega_L \simeq 17$ meV)[29,30]. Here $\varepsilon(\infty)$ represents the dielectric constant below band gap, which is the summation of the low-energy tail of higher-lying electronic excitations. The decrease of band gap generally increases $\varepsilon(\infty)$. Therefore, we attribute the enhancement of the Born effective charge to the band gap closing, at which the topological transition into, for example, the Weyl semimetal phase, is predicted. The robust low-energy phonon produces the large dielectric response with assist of band gap closing in the present ferroelectric semiconductors. We note that although it is difficult to indicate the actual boundary of the Weyl semimetal phase at the current stage, the enhancement of mobility, SHG and dielectric constant infer the emergence of Weyl semimetal phase around x ~ 0.16 – 0.3[25].

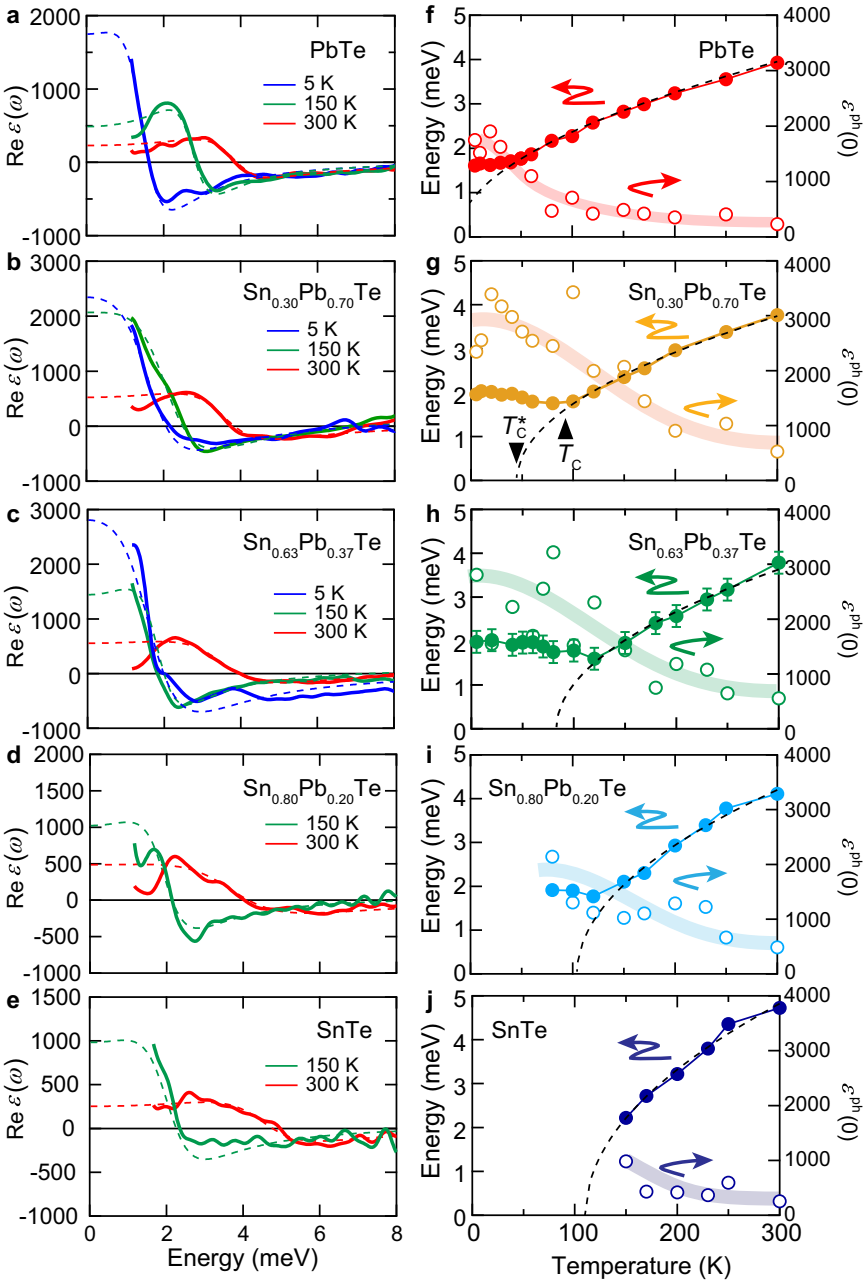

Fig. 4 Terahertz phonon dynamics. a–e Selected terahertz in-plane dielectric spectra Re $\varepsilon(\omega)$ for $Sn_xPb_{1-x}Te$ ($x = 0$, 0.30, 0.63, 0.80, and 1). The dotted curves are fits with Re $\varepsilon^{ph}(\omega)$ in Eq. (2). **f–j** Temperature dependence of the TO phonon energy ω_T obtained from fits with Eqs. (1) and (2) (filled circles) and DC dielectric constant arising from the soft TO phonons Re $\varepsilon(\omega = 0)$ (open circles). The dotted curves represent the Curie Weiss law. The definitions of T_C^* and T_C are indicated in (**g**) as an example. The thick curves are the guide to the eyes. The error bars in (**h**) is roughly estimated from the width of artificial fringe in spectra.

DISCUSSION

In summary, we have investigated the terahertz response of the ferroelectric semiconductor $Sn_xPb_{1-x}Te$. By combining the terahertz time-domain spectroscopy and finely controlled thin films, we can address the quantitative evaluation of the terahertz conductivity and dielectric spectra. We observe the coexistence of the clear TO phonon excitation and the electronic continuum band in the terahertz conductivity spectra, which can be decomposed by the simple model analysis. The TO phonon shows the softening and then slightly hardening irrespective of the change in the DC conductivity depending on the composition. This observation indicates the ferroelectric transition relatively robust against the presence of conduction electrons, providing the direct evidence for the polar semiconductor in this system. The putative phase diagram obtained from the terahertz spectroscopy suggests the stabilization of the ferroelectric phase compared with the bulk crystals possibly due to compressive strain characteristic of the thin films. It is also found that the large DC dielectric constant induced by the TO phonon is further enhanced at around $x = 0.3$ owing to the band gap closing; such enhancement of the dielectric response could be generally expected for the polar topological semimetal system. Our systematic terahertz spectroscopy establishes the lattice dynamics in polar semiconductors, which should be directly coupled to the stability of the topological phases, especially the Weyl semimetal phase. The present results suggest that the thin film with high

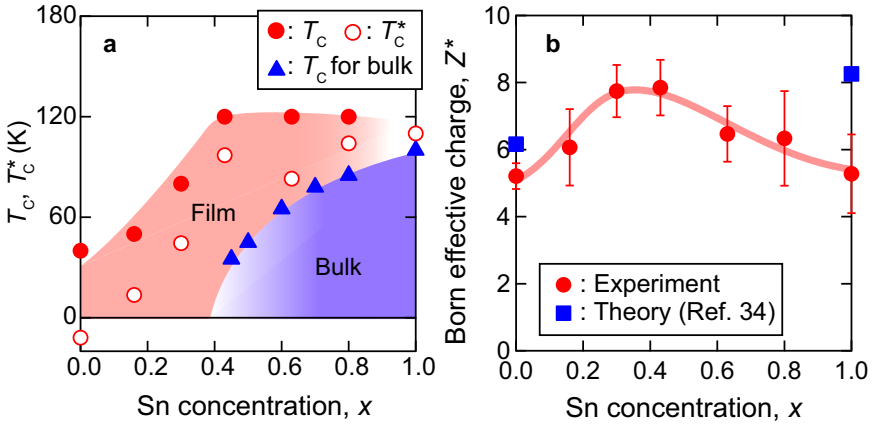

Fig. 5 Ferroelectric phase diagram and enhancement of Born effective charge. a The ferroelectric phase diagram determined from the phonon spectroscopy. The red filled and open circles respectively represent T_C and T_C^* (see main text for definition). The blue filled triangles are the transition temperature for the bulk system taken from refs. [15,33,35]. While the T_C depends on the carrier concentration at least for bulk SnTe, we plot the highest T_C reported in ref. [15]. **b** The x dependence of the Born effective charge Z^*. The red circles and blue squares denote the experimental values and theoretical ones from the first-principles calculation[34], respectively. The vertical bars represent the thermally induced variation, which is defined as the standard deviation of the Z^* calculated at each temperature (See also Supplementary Fig. 3). The red thick curve is the guide to the eyes.

tunability of composition and strain field provides the ideal platform to control of the versatile topological phases beyond the bulk crystal. Last but not least, we note that the observed TO phonon is theoretically suggested to lower the energy of the valence band maximum and increase the energy of the conduction band minimum, particularly along the L–W line via the Jones-Peierls mechanism in terms of the first-principles calculation[21]. Since the topological transition occurs at the L point[12], the intense excitation of the TO phonon with a large dielectric response may open a new route for the ultrafast optical control of the topological electronic states including the Dirac surface state and Weyl semimetallic states.

METHODS

Sample fabrication and characterization of transport properties

We fabricated 40-nm thick (111)-oriented (Sn,Pb)Te epitaxial thin films on InP(111)A substrate by molecular beam epitaxy. The epi-ready substrate was annealed at 350 °C in a vacuum before the epitaxy and then set to 400 °C to grow the thin film. We inserted 2-nm thick SnTe buffer layers beneath the (Sn,Pb)Te layer, which helps to stabilize (111) orientation of (Sn,Pb)Te thin films. The growth temperature of the buffer layer was also 400 °C. We set the equivalent pressures of Sn and Te for the buffer layer at $P_{Sn} = 5.0 \times 10^{-6}$ Pa and $P_{Te} = 1 \times 10^{-4}$ Pa, respectively. For the (Sn,Pb)Te layer, we keep the sum of the equivalent beam pressures of Sn and Pb as $P_{Sn} + P_{Pb} = 1 \times 10^{-5}$ Pa, and change their ratio to change the Pb composition. We calibrated the actual Pb composition by inductively coupled plasma mass spectroscopy and defined it as x in the main text. The calibrated x value was larger than the nominal one by 0.1 ~ 0.2. The growth duration of the SnTe buffer layer and (Sn,Pb)Te layer was respectively 2 and 30 min regardless of x. These conditions are the same as the previous study reporting the transport properties and SHG[25]. We measured the transport properties using the standard four-terminal method by the Physical Properties Measurement System (PPMS, Quantum Design). The transport property is reproducible for fabricated thin film and all the physical quantities show the systematic variation against the composition. Therefore, it is possible to discuss the polar nature based on the SHG and the present terahertz experiments.

Terahertz time-domain spectroscopy

The laser pulses with a duration of 100 fs from a mode-locked Ti:sapphire laser were split into two paths to generate and detect the terahertz light by using the photoconductive antenna. The complex transmission spectrum $t(\omega)$ is obtained by comparing the Fourier transformation of the electric-field transmission through the (Sn,Pb)Te/InP and InP substrate. We then deduced the terahertz conductivity spectra $\sigma(\omega)$ from the following standard formula; $t(\omega) = (1 + n_s) / (1 + n_s + Z_0 d\sigma(\omega))$, where d, Z_0, and n_s are the thickness of the film, the vacuum impedance (377 Ω), and the refractive index of the InP substrate, respectively. We note that the optical response from the buffer layer is negligible (for details, see Supplementary Fig. 4).

DATA AVAILABILITY

The data that support the plots of this study are available from the corresponding author upon reasonable request.

Received: 9 March 2022; Accepted: 30 August 2022;
Published online: 10 September 2022

REFERENCES

1. Scott, J. F. Application of modern ferroelectrics. *Science* **315**, 954–959 (2007).
2. Shi, Y. et al. A ferroelectric-like transition in a metal. *Nat. Mater.* **12**, 1024–1027 (2013).
3. Kolodiazhnyi, T., Tachibana, M., Kawaji, H., Hwang, J. & Takayama-Muromachi, E. Persistence of ferroelectricity in $BaTiO_3$ through the insulator-metal transition. *Phys. Rev. Lett.* **104**, 147602 (2010).
4. Fujioka, J. et al. Ferroelectric-like metallic state in electron doped $BaTiO_3$. *Sci. Rep.* **5**, 13207 (2015).
5. Fei, Z. et al. Ferroelectric switching of a two-dimensional metal. *Nature* **560**, 336–339 (2018).
6. Sharma, P. et al. A room-temperature ferroelectric semimetal. *Sci. Adv.* **5**, eaax5080 (2019).
7. Anderson, P. W. & Blount, E. I. Symmetry considerations on martensitic transformations: "ferroelectric" metals? *Phys. Rev. Lett.* **14**, 217–219 (1965).
8. Sie, E. J. et al. An ultrafast symmetry switch in a Weyl semimetal. *Nature* **565**, 61–66 (2019).
9. Sakai, H. et al. Critical enhancement of thermopower in a chemically tuned polar semimetal $MoTe_2$. *Sci. Adv.* **2**, e1601378 (2016).

10. Tanaka, Y. et al. Experimental realization of a topological crystalline insulator in SnTe. *Nat. Phys.* **8**, 800–803 (2012).
11. Xu, S.-Y. et al. Observation of a topological crystalline insulator phase and topological phase transition in $Pb_{1-x}Sn_xTe$. *Nat. Commun.* **3**, 1192 (2012).
12. Hsieh, T. H. et al. Topological crystalline insulators in the SnTe material class. *Nat. Commun.* **3**, 982 (2012).
13. Pawley, G. S., Cochran, W., Cowley, R. A. & Dolling, G. Diatomic ferroelectrics. *Phys. Rev. Lett.* **17**, 753–755 (1966).
14. O'Neill, C. et al. Inelastic x-ray investigation of the ferroelectric transition in SnTe. *Phys. Rev. B* **95**, 144101 (2017).
15. Kobayashi, K. L. I., Kato, Y., Katayama, Y. & Komatsubara, K. F. Carrier-concentration-dependent phase transition in SnTe. *Phys. Rev. Lett.* **37**, 772–774 (1976).
16. Wood, C. Materials for thermoelectric energy conversion. *Rep. Prog. Phys.* **51**, 459–539 (1988).
17. Nolas, G. S., Sharp, J. & Goldsmid, H. J. Thermoelectrics, Basic Principles and New Materials Developments (Springer, 2001).
18. Delaire, O. et al. Giant anharmonic phonon scattering. *Nat. Mater.* **10**, 614–619 (2011).
19. Bozin, E. S. et al. Entropically stabilized local dipole formation in lead chalcogenides. *Science* **330**, 1660–1663 (2010).
20. Li, C. W. et al. Phonon self-energy and origin of anomalous neutron scattering spectra in SnTe and PbTe thermoelectrics. *Phys. Rev. Lett.* **112**, 175501 (2014).
21. Jiang, M. P. et al. The origin of incipient ferroelectricity in lead telluride. *Nat. Commun.* **7**, 12291 (2016).
22. Murakami, S., Hirayama, M., Okugawa, R. & Miyake, T. Emergence of topological semimetals in gap closing in semiconductors without inversion symmetry. *Sci. Adv.* **3**, e1602680 (2017).
23. Liang, T. et al. A pressure-induced topological phase with large Berry curvature in $Pb_{1-x}Sn_xTe$. *Sci. Adv.* **3**, e1602510 (2017).
24. Zhang, C. L. et al. Highly tunable topological system based on PbTe-SnTe binary alloy. *Phys. Rev. Mater.* **4**, 091201 (2020).
25. Yoshimi, R. et al. Versatile electronic states in epitaxial thin films of (Sn-Pb-In)Te: from topological crystalline insulator and polar semimetal to superconductor. *Phys. Rev. Mater.* **5**, 094202 (2021).
26. Zhang, C. L. et al. Berry curvature generation detected by Nernst responses in ferroelectric Weyl semimetal. *Proc. Natl. Acad. Sci.* **118**, e2111855118 (2021).
27. Suzuki, N. & Adachi, S. Optical properties of PbTe. *Jpn. J. Appl. Phys.* **33**, 193–198 (1994).
28. Suzuki, N. & Adachi, S. Optical properties of SnTe. *Jpn. J. Appl. Phys.* **34**, 5977–5983 (1995).
29. Brillson, L. J., Burstein, E. & Muldawer, L. Raman observation of the ferroelectric phase transition in SnTe. *Phys. Rev. B* **9**, 1547–1551 (1974).
30. Wu, H. et al. Observation of phonon modes in epitaxial PbTe films grown by molecular beam epitaxy. *J. Appl. Phys.* **101**, 103505 (2007).
31. Scott, J. F. Soft-mode spectroscopy. *Rev. Mod. Phys.* **46**, 83 (1974).
32. Feder, J. & Pytte, E. Theory of a structural phase transition in perovskite-type crystals. II. *Interact. elastic strain. Phys. Rev. B* **1**, 4803–4810 (1970).
33. Bussmann-Holder, A. Interplay of polarizability and ionicity in IV-VI compounds. *Phys. Rev. B* **40**, 11639–11643 (1989).
34. Waghmare, U. V., Spaldin, N. A., Kandpal, H. C. & Seshadri, R. First-principles indicators of metallicity and cation off-centricity in the IV-VI chalcogenides of divalent Ge, Sn, and Pb. *Phys. Rev. B* **67**, 125111 (2003).
35. Nimtz, G. & Schlicht, B. Narrow Gap Semiconductors, Vol. 98 of Springer Tracts in Modern Physics, edited by G. Hohler (Springer, New York, 1983), and references therein.

ACKNOWLEDGEMENTS

We thank J. Fujioka for fruitful discussion. This work is partly supported by JSPS/MEXT Grant-in-Aid for Scientific Research (No. 21H01796), and JST CREST (No. JPMJCR1874).

AUTHOR CONTRIBUTIONS

Y. Tokura and Y. Takahashi conceived the project. Y.O. and H.H. performed the terahertz measurement and analyzed the data. R.Y. fabricated the thin films under supervision of A.T., K.S.T., M.K. and Y. Tokura. Y.O., H.H., R.Y., Y. Tokura and Y. Takahashi discussed and interpreted the results with inputs from other authors. Y.O. and Y. Takahashi wrote the manuscript with the assistance of other authors.

COMPETING INTERESTS

The authors declare no competing interests.

ADDITIONAL INFORMATION

Supplementary information The online version contains supplementary material available at https://doi.org/10.1038/s41535-022-00501-2.

Correspondence and requests for materials should be addressed to Y. Okamura or Y. Takahashi.

Reprints and permission information is available at http://www.nature.com/reprints

Publisher's note Springer Nature remains neutral with regard to jurisdictional claims in published maps and institutional affiliations.